Supplementary Information

Tailoring the cage and functionality of POSS for scalable low-dielectric and tough cyanate ester hybrid resin

Zongwu Zhang [a], Yijie Zhou a, Yikang Cao [a], Xutao Ma [a], Shumeng Wang [a], Jian Wang [a], Ziqian Xiang [a], Fang Chen [a], Xiaoyan Ma [a, *]

a School of Chemistry and Chemical Engineering, Northwestern Polytechnical University, Xi'an 710072, PR China

*** Correspondence**: Xiaoyan Ma, School of Chemistry and Chemical Engineering, Northwestern Polytechnical University, Xi'an 710072, PR China. Email: m_xiao_yana@nwpu.edu.cn

S1 Materials

Trimethoxyphenylsilane (KH550, Shanghai Maclean Biochemical Technology Co., Ltd., 95%); Sodium hydroxide (NaOH, Shanghai Aladdin Biochemical Technology Co., Ltd., ≥ 98%); Dichloromethylsilane (DCMS, Shanghai Maclean Biochemical Technology Co., Ltd., 97%); Dimethylchlorosilane (DMCS, Shanghai Maclean Biochemical Technology Co., Ltd., 96%); Triethylamine (TEA, Shanghai Maclean Biochemical Technology Co., Ltd., 99%); Eugenol (EG, Shanghai Maclean Biochemical Technology Co., Ltd., 99%); Epichlorohydrin (ECH, Shanghai Maclean Biochemical Technology Co., Ltd., AR), Sodium carbonate anhydrous (Na_2CO_3, Shanghai Maclean Biochemical Technology Co., Ltd., 99.5%); Karstedt Catalyst Solution (Pt: ~2%, in xylene); Toluene (Chengdu Kelong Chemical Co., Ltd., > 99.9%); Tetrahydrofuran (THF, Chengdu Kelong Chemical Co., Ltd., > 99.5%), Petroleum ether (PE, Chengdu Kelong Chemical Co., Ltd., > 99.5%); Isopropanol (IPA, Chengdu Kelong Chemical Co., Ltd., > 99.5%); silica gel (Greagent, 200–300 mesh). Bisphenol A-type cyanate ester resin (CE, 1.171 g/cm^3, Jiangsu Wuqiao Resin Factory Co., Ltd.); Toluene THF and acetone used for reactions were dried through a solvent purification system (SPS-5, Etelux, Beijing, China). Deionized water was obtained in our lab; All other chemicals were used as received without further purification.

S2 Measurements

^{1}H-NMR, ^{13}C-NMR and ^{29}Si-NMR spectra were recorded on a Bruker ANANCE-400MHz NMR instrument using $CDCl_3$ as solvent.

Fourier transform infrared (FTIR) spectra were measured by Bruker TENSOR 27(Germany) with the wavenumber range of 400-4000 cm^{-1}.

MALDI-TOF mass spectrum were recorded on an ultraflextreme MALDI TOF/TOF Mass Spectrometer (Bruker Daltonics) in positive reflection mode.

The pore size distribution of 2(or 4)EGEP-POSS was measured by the BET (Brunauer-Emmet-Teller) method through the N_2 adsorption-desorption instrument (Tristar 3020, Micromeritics) to evaluate the cage-size order.

DSC was performed on a PerkinElmer DSC 8000 under nitrogen atmosphere with heating rates of 10 °C min^{-1}.

Xray photoelectron spectroscopy (XPS, Kratos AXIS Ultra DLD) was used to analyze material element valences.

UV–vis spectra were performed on a UV-1800PC (Shanghai Mapada Co., Ltd.).

The $(\alpha h\nu)^2$-hν plots of CE, CE/2(or 4)EGEP-POSS samples are converted from the UV-vis spectrum by Tauc plot, where the α, h, and ν are the absorption coefficient, Planck constant, and light frequency, respectively. The energy band gap (Eg) was determined through the absorption onset of the linear region[1, 2].

WAXD measurement was recorded on an X'pert pro MPD X-ray diffractometer (PANalytical B.V., Holland) with a Cu Kα radiation (40 kV, 40 mA).

The morphology of CE/2(or 4)EGEP-POSS samples were observed by transmission electron microscope (TEM, FEI Talos F200X, U.S.A). The corresponding CE/POSS slices were cut at room temperature by LEICA UC7 freezing microtome and stained by osmium tetroxide (OsO4) for two hours.

Dynamic Mechanical Analysis (DMA) scans were performed using DMA/SDTA861e apparatus. DMA tests were carried out from 50 °C to 350 °C with a heating rate of 3.0 °C/min at 1 Hz. The sample dimension was (50 ± 0.02) × (10 ± 0.02) × (4 ± 0.02) mm^3.

Crosslinking density (ρ) of the samples was calculated by equation of rubbery elasticity: $\rho = \frac{E'}{2(1+\gamma)RT}$, where γ is Poisson's ratio assumed as 0.5 for incompressible networks; R is gas constant, T is related to Tg + 40 °C and E' is the storage modulus of materials at Tg + 40 °C.

Thermal gravimetric analysis (TGA) was performed by STA 449F3 (NETZSCH Co., Germany) thermal gravimetric analyzer. The test temperature range was 40-800 ℃, and the heating rate was 10 ℃/min under nitrogen atmosphere.

The impact strength and flexural strength of resins were measured according to the ISO 179-2010 standard and ISO 178-2010 standard by a ZBC 1000 pendulum impact tester from MTS Industrial Systems Co., Ltd (China) and CMT6303 electronic universal testing machine of Xinsansi Material Testing Co., Ltd (Shenzhen, China), respectively. The impact profile analysis was carried out using VEGA 3 LMH scanning electron microscope (SEM) from Tesken Trading Co., Ltd (Czech), and the accelerating voltage was 10KV.

Dielectric constant (k) and dielectric loss tangent (tanδ) values of the samples were measured using a Novocontrol Concept 80 broad frequency dielectric spectrometer with a frequency ranging from 10 Hz to 1 MHz. Whereas their high-frequency dielectric properties were texted by a Vector Network Analyzer with a frequency ranging from 8.2 Hz to 10.2 GHz.

Density functional theory (DFT) calculations were carried out at B3LYP/6-31G(d) level using Gaussian 09 program.

Contact angles of samples with water were measured using a DSA100 contact angle measuring device at room temperature and the volume of each water droplet was controlled at 2 μL.

The microwave transmittances of the samples were calculated by the theoretical microwave-transmission mold[3, 4]:

$$A = \frac{2\pi dk\ tan\delta}{\lambda(\delta - sin^2\theta)^{1/2}} \quad (2)$$

$$\Gamma = \frac{(k - sin^2\theta)^{1/2} - \varepsilon\ cos\theta}{(k - sin^2\theta)^{1/2} + \varepsilon\ cos\theta} \quad (3)$$

$$\left|T\right|^2 = 1 - A - \left|\Gamma\right|^2 \quad (4)$$

Where λ represents the length of electromagnetic waves; $\theta = 0\circ$ represents the incident angle of the electromagnetic wave on the surface of the composites; $d = 1$ mm represents the thickness of material; A, $\left|\Gamma\right|^2$ and $\left|T\right|^2$ represent the energy loss, reflection coefficient, and wave transmission efficiency when electromagnetic waves pass through the material.

The simulation model of the spherical nose-cone radome is constructed by using the EastWave7.6 software based on the methods of the full-wave finite-difference Timedomain (FDTD) and high-frequency physical optics (PO) to further verify electromagnetic wave transmission (phase difference and power transmission coefficient) of the practical application scene. The wall thickness, top sphere radius, half cone angle, and height of the radome model are 1.5 mm, 20.0 mm, 20.0° and 240.0 mm, respectively.

S3 Synthesis of Eugenol-epoxy and DDSQ-type cage

Eugenol-epoxy was synthesized via the classic "Williamson Mechanism" according to literature. Typically, in a three-necked flask (250 mL), Eugenol (32.8 g, 200 mmol), Potassium carbonate (33.2 g, 240 mmol) and Epichlorohydrin (92.5 g, 1000 mmol) were added under nitrogen atmosphere. Then, the mixture was heated to 120 ℃ and reacted for 24 hours. After cooling to room temperature, the organic phase was washed with deionized water and concentrated under reduced pressure. The crude product was purified by using flash column chromatography on silica gel with THF/PE as eluent to afford 28.2 g product as needle-like crystals. Yield: 64%.

DDSQ-type cage $Na_4O_{14}Si_8(C_6H_5)_8$ was synthesized according to literatures[5, 6]. Typically, KH550 (33.4 g, 160 mmol), deionized water (3.33 g, 185 mmol) and NaOH (4.27 g, 107 mmol) were dissolved in IPA (160 ml) uniformly with a magnetic stirrer. Then the mixture was heated to 85 °C for 4 h and cooled to room temperature for 15 h. After filtering and drying to remove the solvent, 18.3 g products (white powder) was obtained with yield of 77.9%.

2H-POSS was synthesized according to the classical corner capping reaction. Typically, in a three-necked flask (250 mL), $Na_4O_{14}Si_8(C_6H_5)_8$ (11.56 g, 10 mmol), triethylamine (1.52 g, 15 mmol) and anhydrous THF (100 ml) were added at 0 °C and purged by nitrogen for 1 h. Then, dichloromethylsilane (1.73 g, 15 mmol) diluted by 10 ml THF was added slowly within 30 min and the mixture was reacted at room temperature for 24 h. The filtrate was collected and concentrated to recrystallize in methanol. So far, 5.70 g 2H-POSS (white solids) was obtained

with the yield of 48.5%.

4H-POSS was synthesized via nucleophilic reaction. Typically, in a 250 mL three-necked flask, dimethylchlorosilane (7.56 g, 80 mmol), triethylamine (4.04 g, 40 mmol) and anhydrous THF (100 ml) were added at 0 °C under N_2 atmosphere. Then, $Na_4O_{14}Si_8(C_6H_5)_8$ (11.56 g, 10 mmol) was added in five times within 30 min. After that, the reaction was carried out at room temperature for 24 h. The filtrate was collected and concentrated to recrystallize in methanol. So far, 6.9 g TH-POSS (white solids) was obtained with yield of 57.1 %.

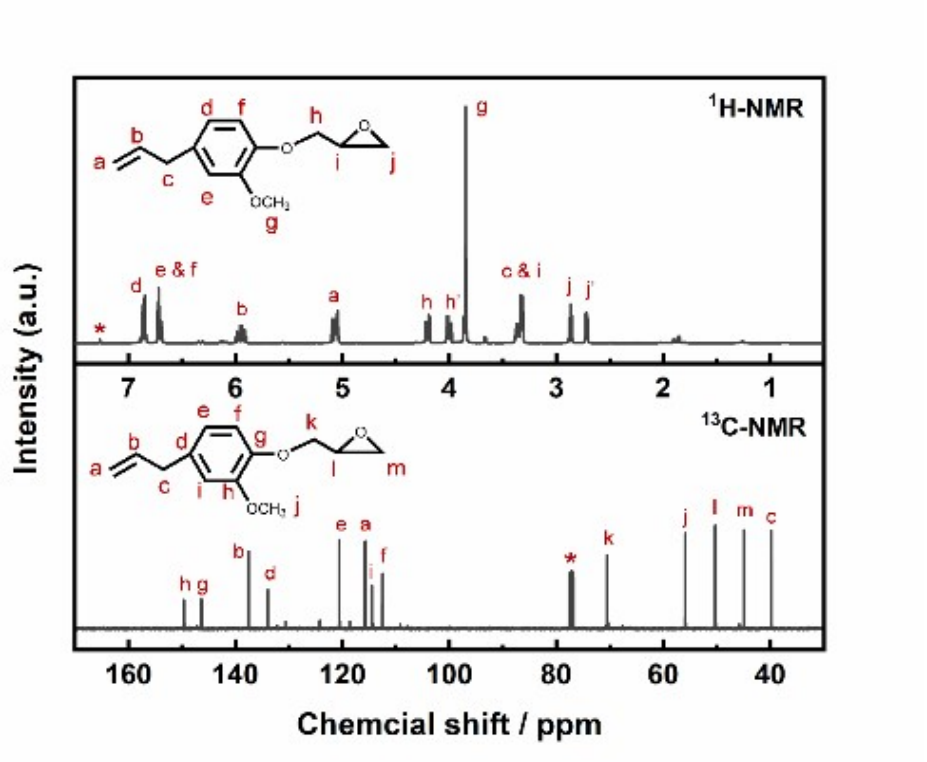

Fig.S1 ^{1}H-NMR and ^{13}C-NMR spectra of eugenol-epoxy (asterisks denote signals from $CDCl_3$, H_2O or THF).

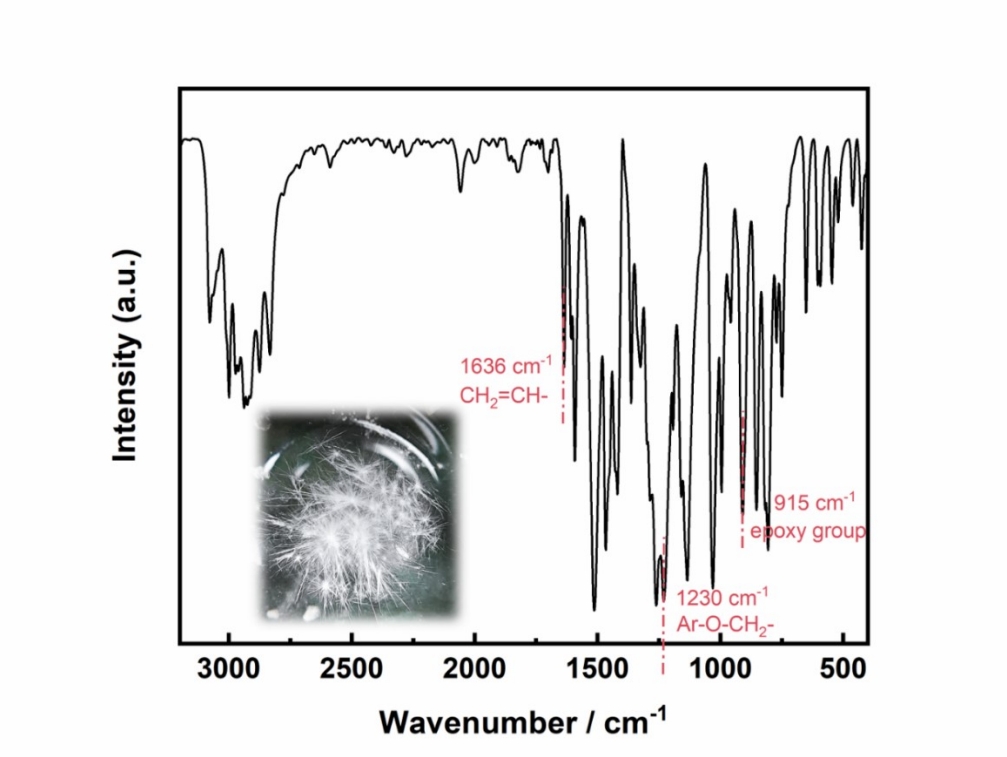

Fig.S2 the Fourier transform infrared (FTIR) spectra of EGEP.

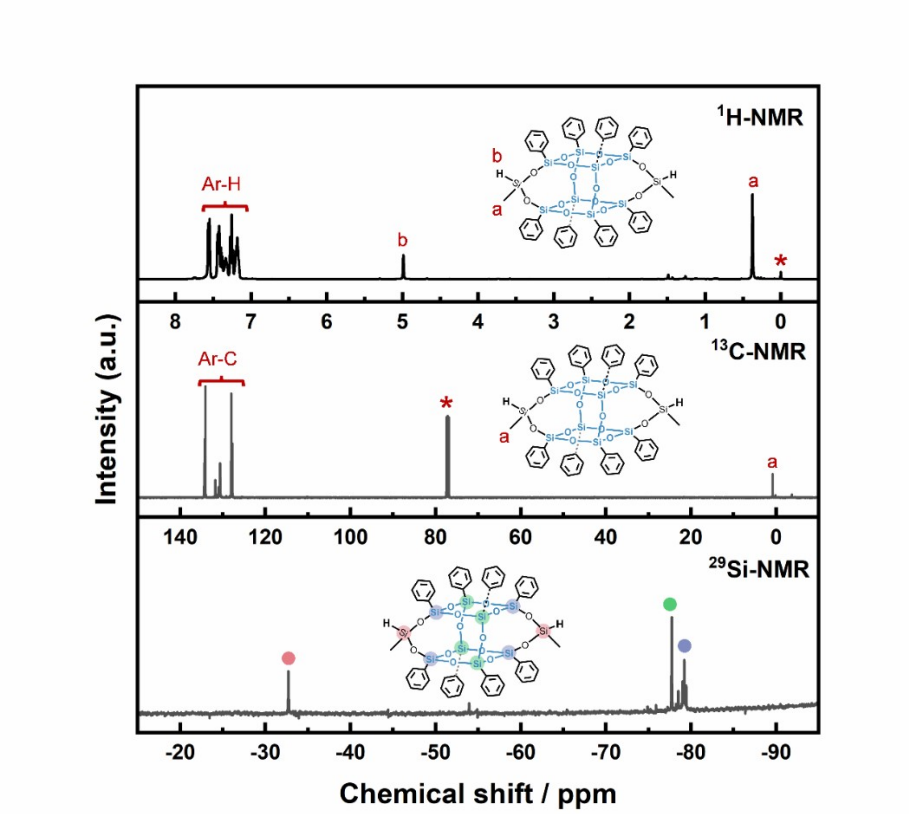

Fig.S3 the ^{1}H-NMR, ^{13}C-NMR and ^{29}Si-NMR spectra of 2H-POSS (asterisks denote signals from $CDCl_3$, H_2O or THF).

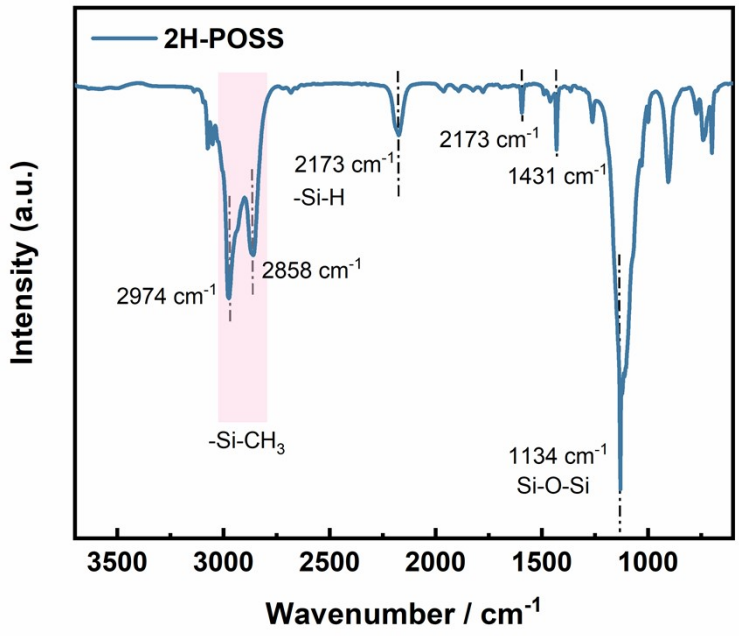

Fig.S4 the Fourier transform infrared (FTIR) spectra of 2H-POSS.

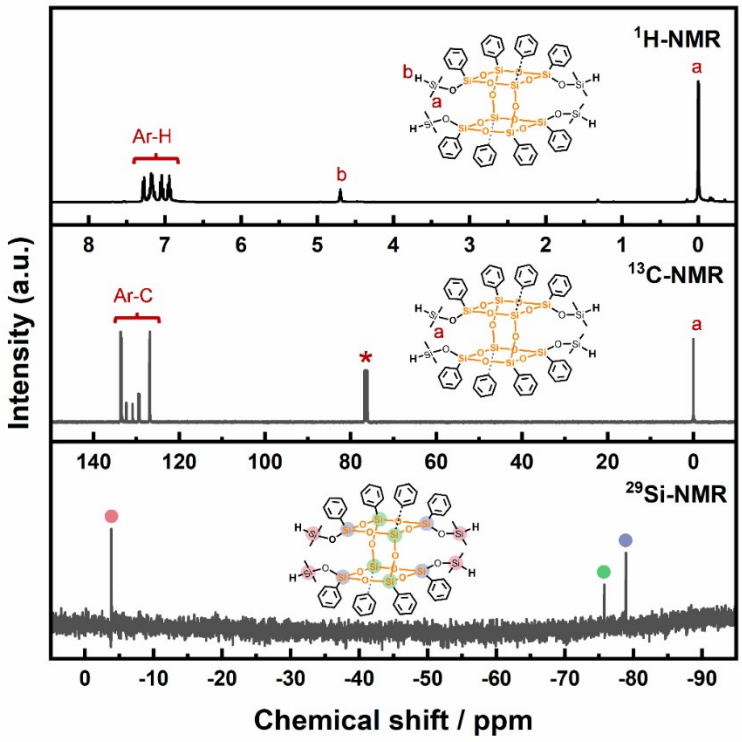

Fig.S5 the ^{1}H-NMR, ^{13}C-NMR and ^{29}Si-NMR spectra of 4H-POSS (asterisks denote signals from $CDCl_3$, H_2O or THF).

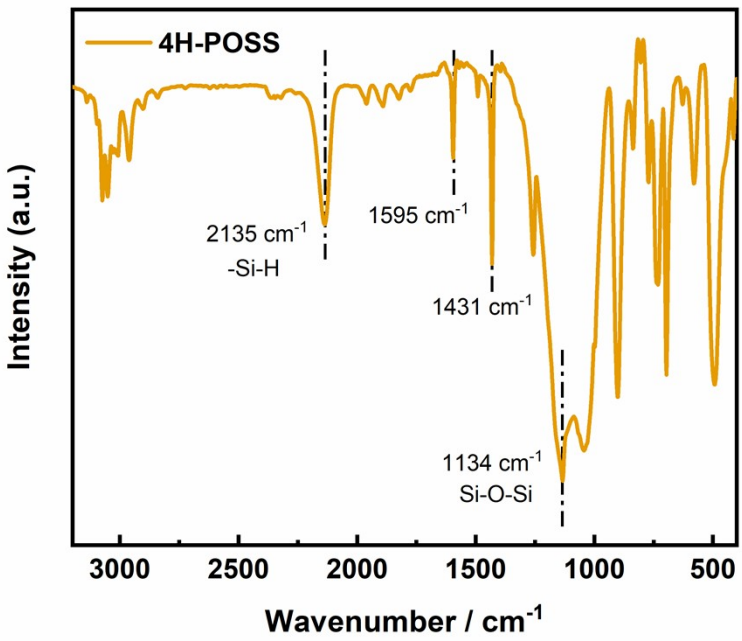

Fig.S6 the Fourier transform infrared (FTIR) spectra of 4H-POSS.

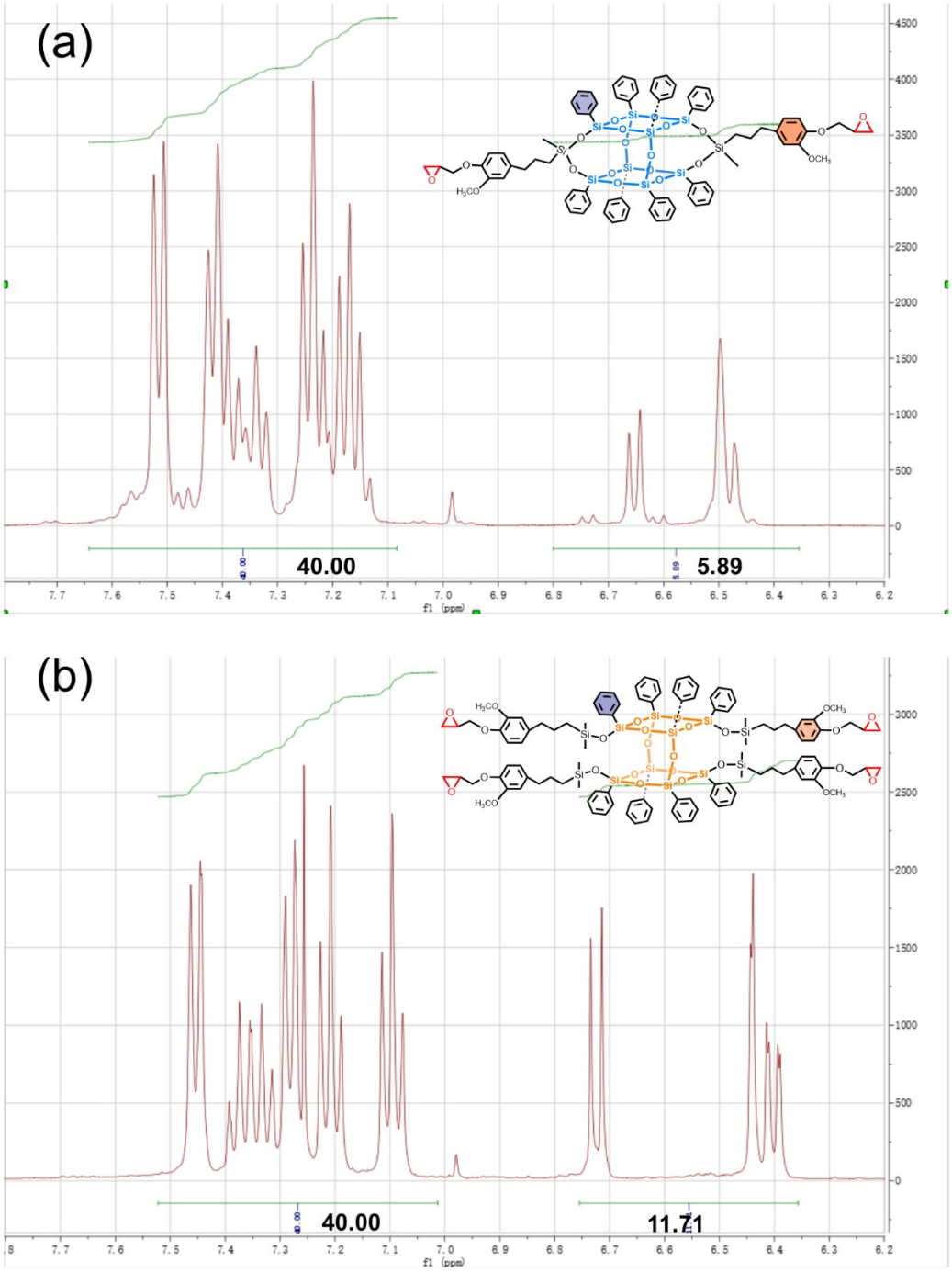

Fig.S7 aromatic ratios (*N*) of EGEP groups to DDSQ-type cage in 2(or 4)EGEP-POSSs according to $N = \frac{n_E/3}{n_D/5}$, where n_D and n_E are the normalized proton numbers of DDSQ cage and EGEP, respectively.

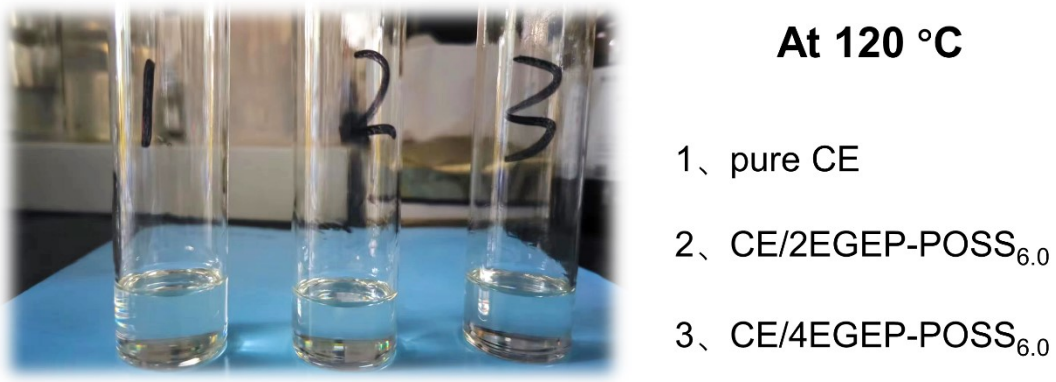

Fig.S8 Optical photograph of the mixture of cyanate ester monomer and 2(or 4)EGEP-POSS under 120 ℃.

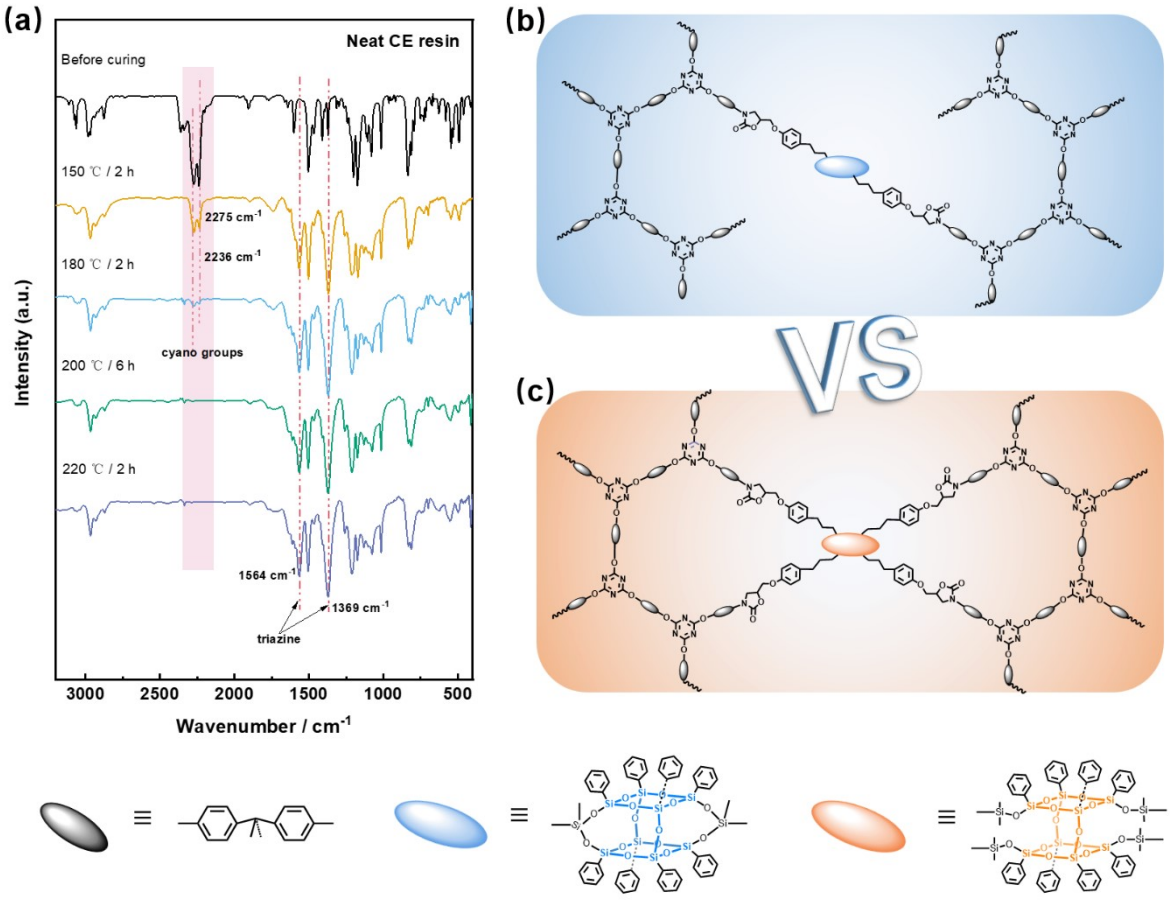

Fig.S9 (a) the online-FTIR spectra of CE; (b & c) schematic diagram of the chemical structures for 2(or 4)EGEP-POSS hybrid resin.

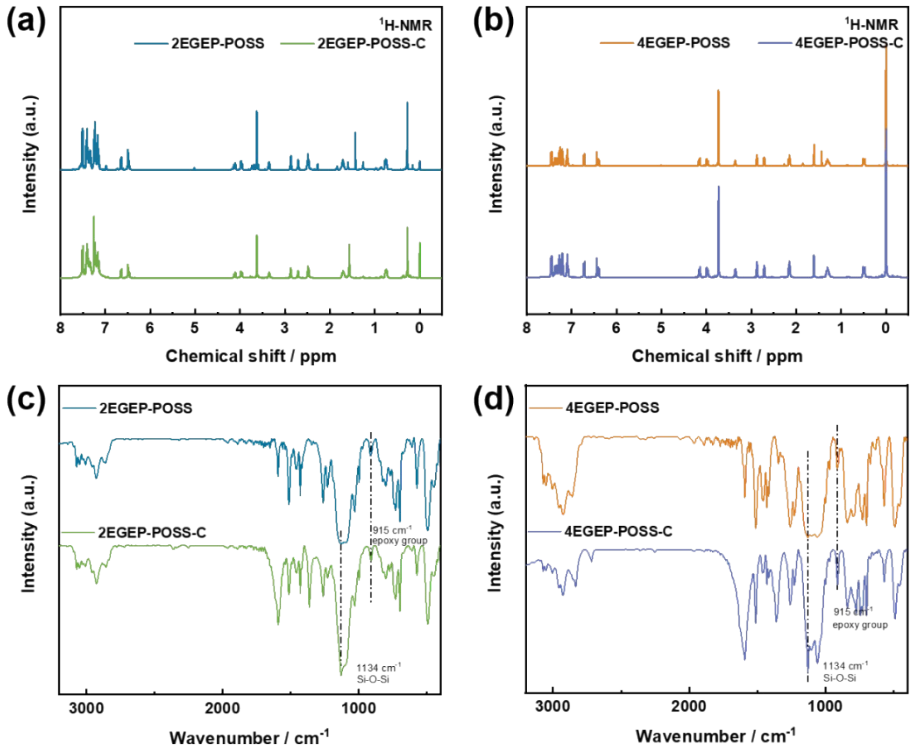

Fig.S10 (a & b) ^{1}H-NMR spectra of 2(or 4)EGEP-POSS and 2(or 4)EGEP-POSS-C; (c & d) FTIR spectra of 2(or 4)EGEP-POSS and 2(or 4)EGEP-POSS-C.

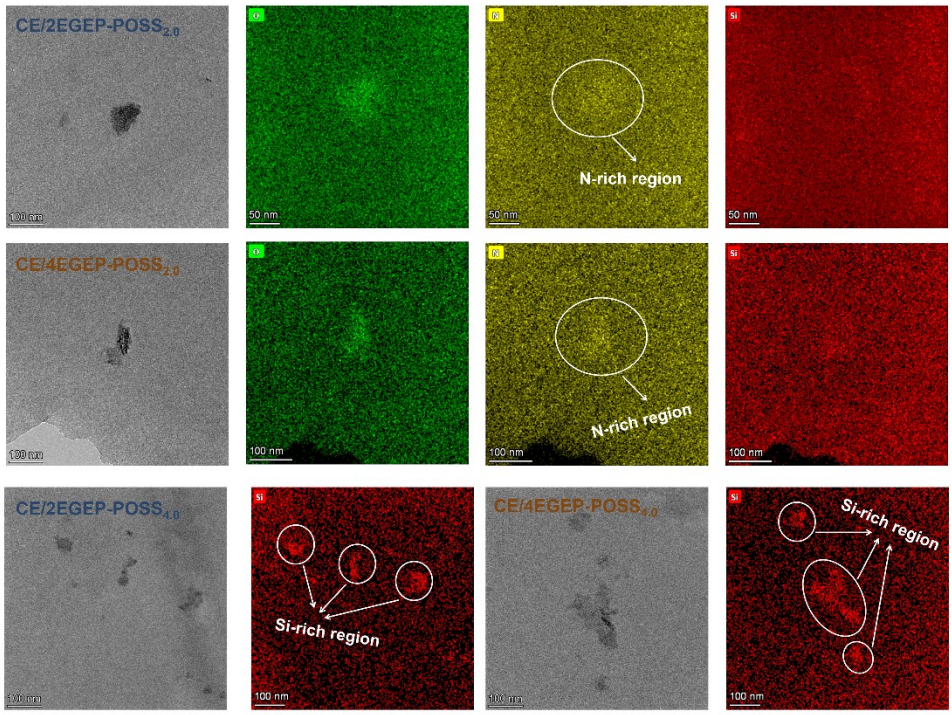

Fig.S11 TEM and EDS mapping of CE/2EGEP-POSS and CE/4EGEP-POSS samples.

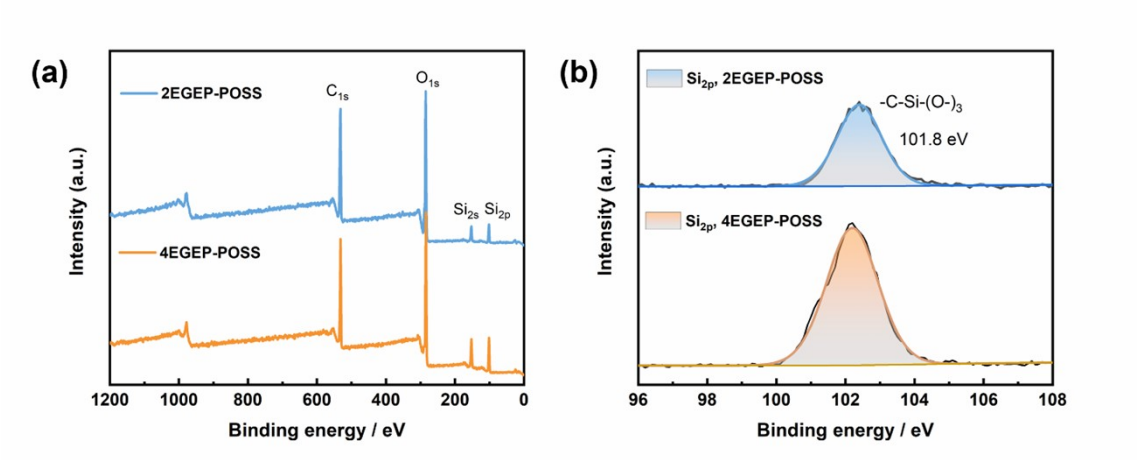

Fig.S12 XPS general spectra (a) and the high-resolution Si2p spectrum (b) of 2EGEP-POSS and 4EGEP-POSS.

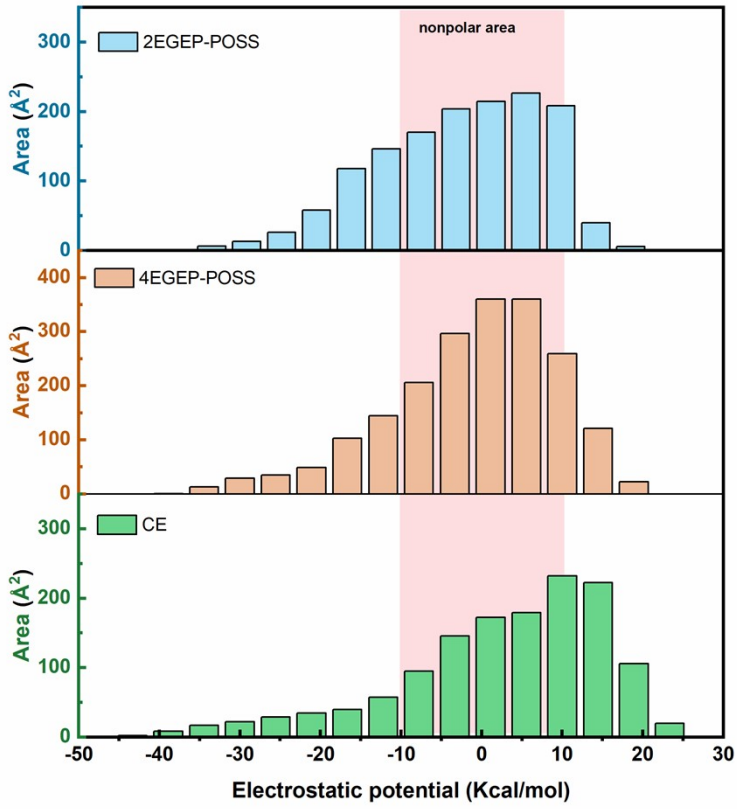

Fig.S13 Electrostatic potential distribution and area percentage in each electrostatic potential range of 2EGEP-POSS, 4EGEP-POSS, and CE.

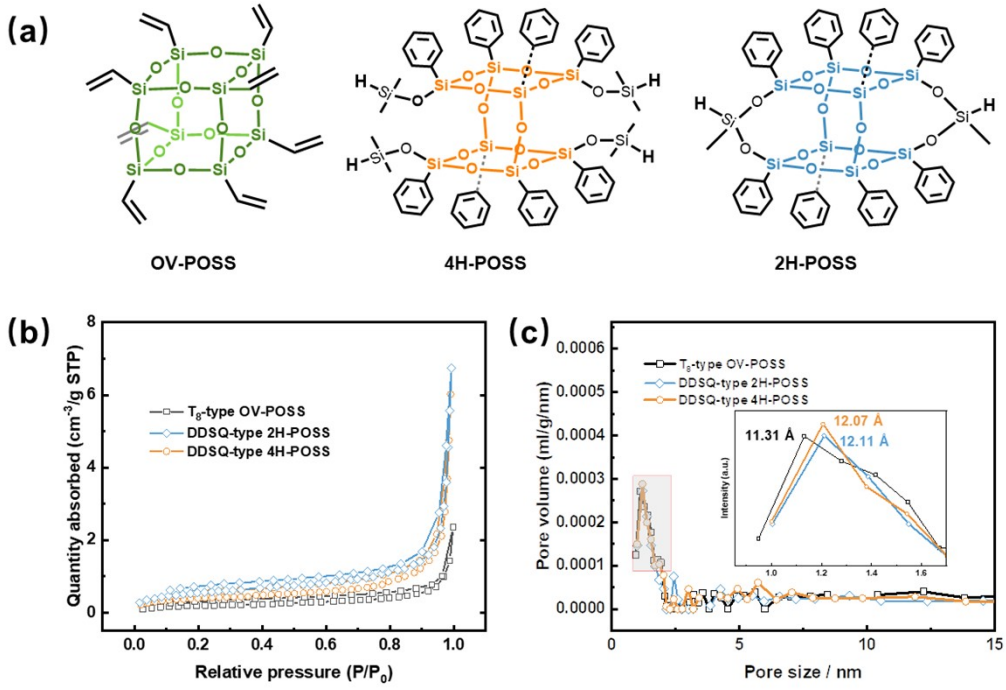

Fig.S14 (a) Structure and (b & c) Nitrogen adsorption-desorption curves of OV-POSS, 2H-POSS and 4H-POSS.

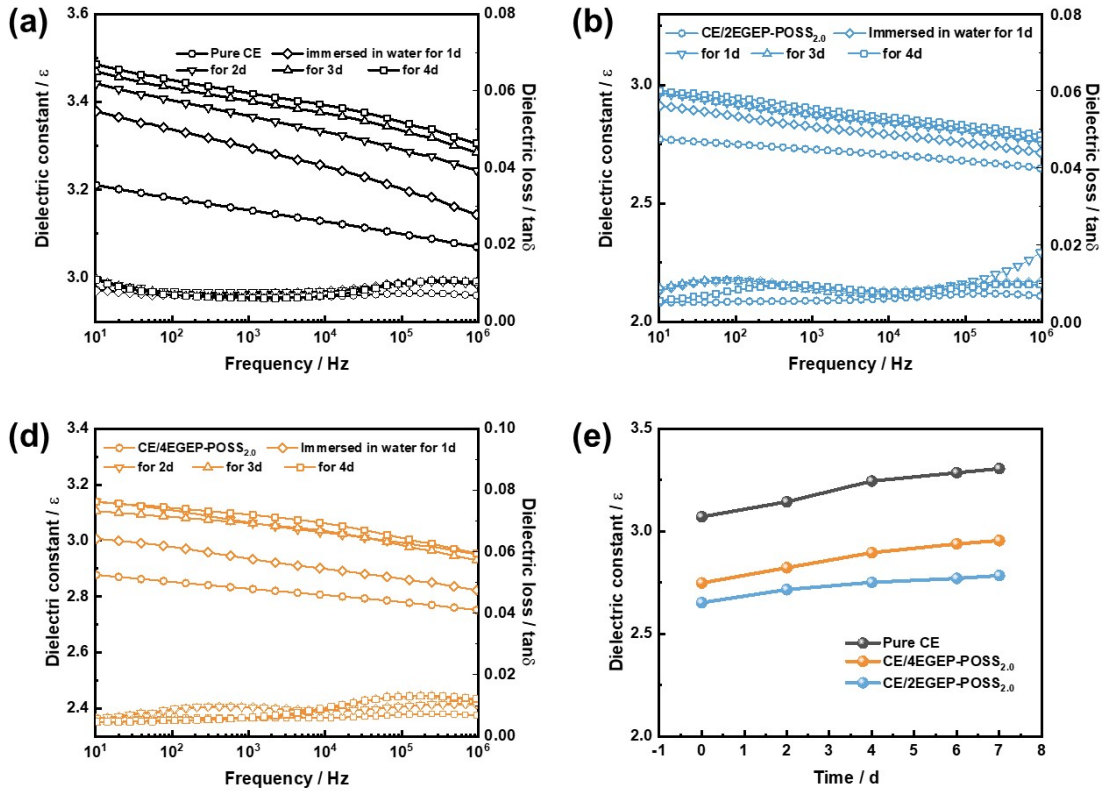

Fig.S15 Broad dielectric spectra of CE, CE/2EGEP-POSS$_{2.0}$ and CE/4EGEP-POSS$_{2.0}$.

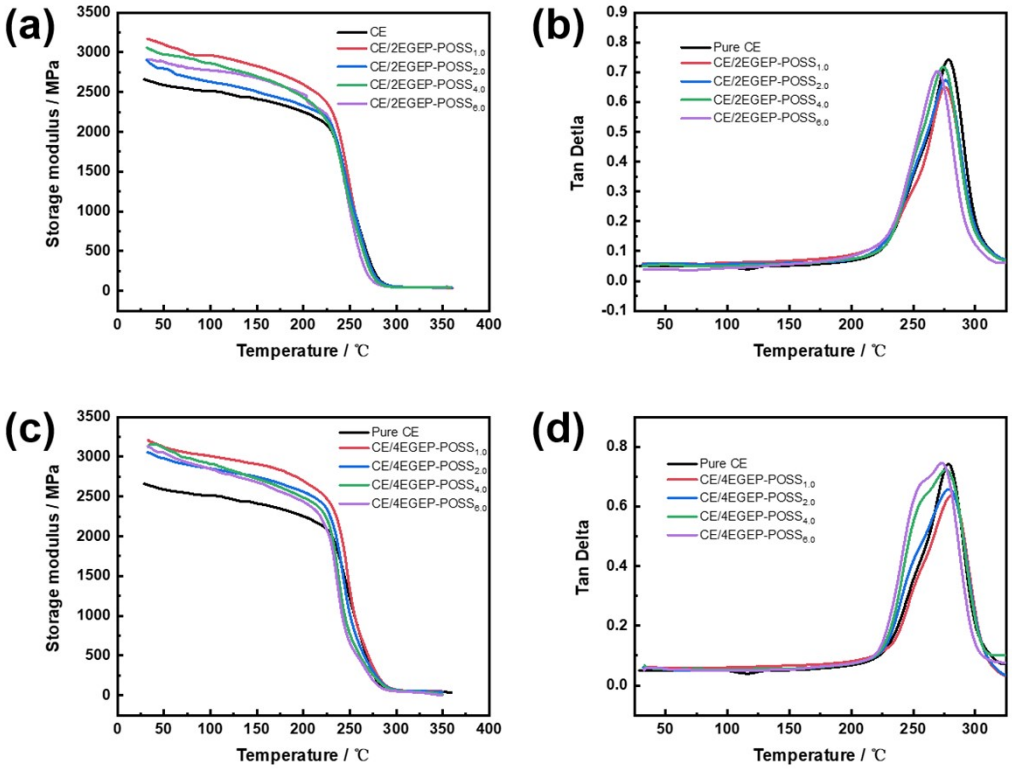

Fig.S16 (a) DMA results of CE/2EGEP-POSS nanocomposites; (b) DMA results of CE/4EGEP-POSS nanocomposites.

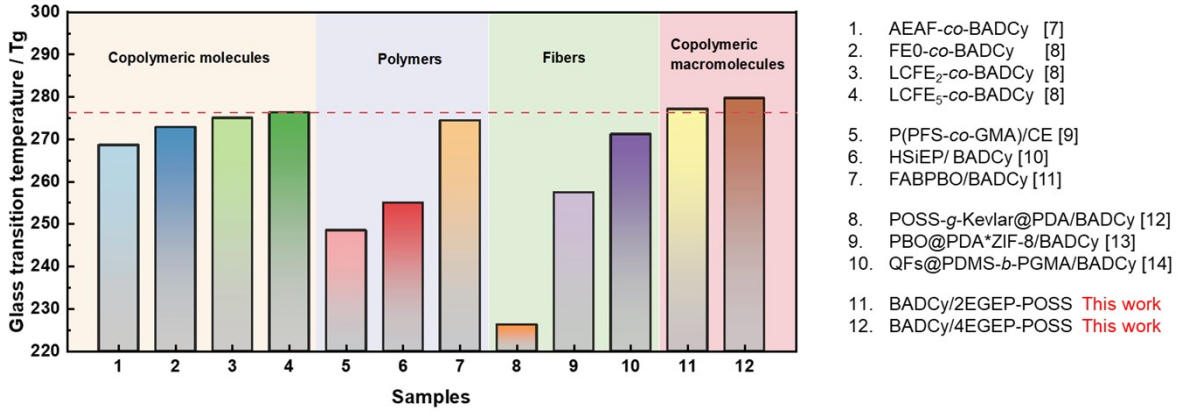

Fig.S17 Comparation of the glass transition temperature of CE/2(or 4EGEP-POSS) in this work and those cyanate ester-based counterparts modified by copolymeric small molecules, linear and hyperbranched polymers, as well as fibers [7-14].

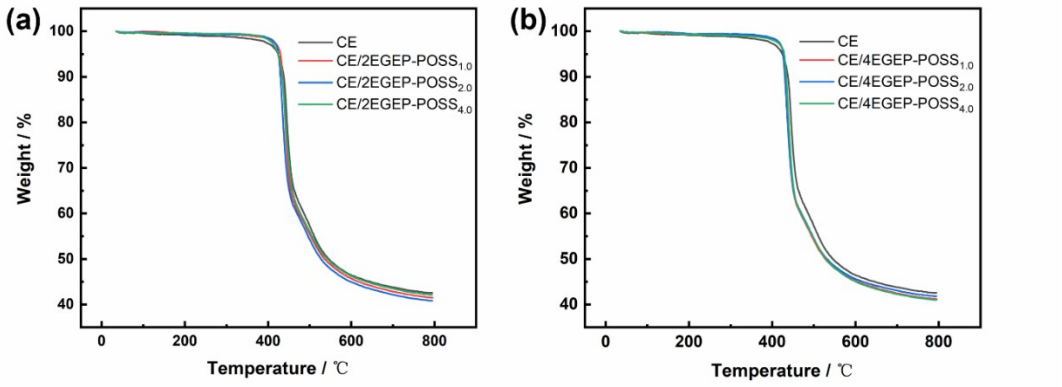

Fig.S18 (a) TGA curves of CE/2EGEP-POSS nanocomposites; (b) TGA curves of CE/4EGEP-POSS nanocomposites.

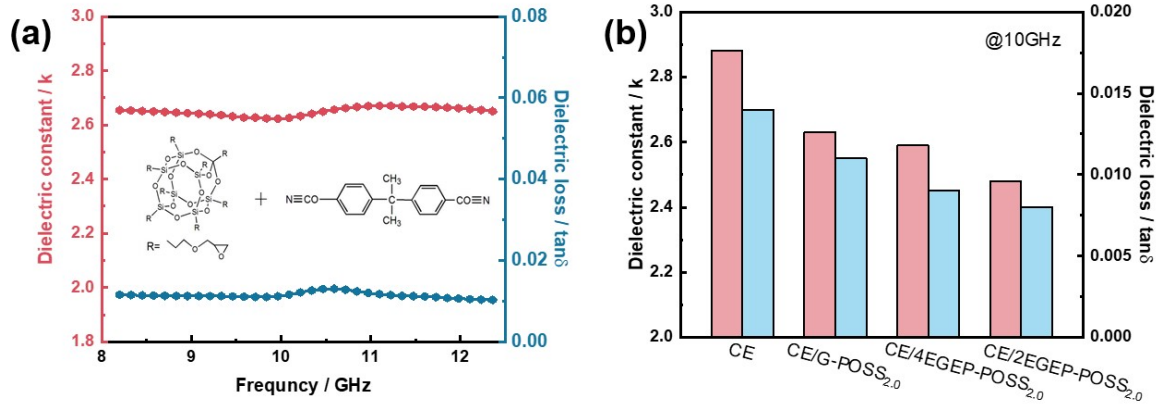

Fig.S19 (a) Curves of dielectric constant and dielectric loss versus frequency for CE/G-$POSS_{2.0}$ hybrid resin at 8.2-10 GHz; (b) the comparation of the dielectric property of CE/G-$POSS_{2.0}$, CE/2EGEP-$POSS_{2.0}$ and CE/4EGEP-$POSS_{2.0}$ hybrid resins at 10 GHz.

Reference

[1] Yang M, Wang Z, Zhao Y, Liu Z, Pang H, Dang ZM. Unifying and suppressing conduction losses of polymer dielectrics for superior high-temperature capacitive energy storage. Adv Mater. 2023.

[2] Dong J, Li L, Qiu P, Pan Y, Niu Y, Sun L, et al. Scalable Polyimide-Organosilicate Hybrid Films for High-Temperature Capacitive Energy Storage. Adv Mater. 2023:e2211487.

[3] Li WC, Huang W, Kang Y, Gong Y, Ying Y, Yu J, et al. Fabrication and investigations of G-POSS/cyanate ester resin composites reinforced by silane-treated silica fibers. Compos Sci Technol. 2019;173:7-14.

[4] Wang CF, Tang YS, Zhou YX, Zhang YY, Kong J, Gu JW, et al. Cyanate ester resins toughened with epoxy-terminated and fluorine-containing polyaryletherketone. Polym Chem-Uk. 2021;12(26):3753-61.

[5] Ma XT, Ji TZ, Ma XY, Zhao XR, Wang WT, Guo HB, et al. Effects of difunctional reactive polyhedral oligomeric silsesquioxane on the properties of EPDM. Journal Of Applied Polymer Science. 2022;139(2).

[6] Wang L, Zhang CY, Zheng SX. Organic-inorganic poly(hydroxyether of bisphenol A) copolymers with double-decker silsesquioxane in the main chains. J Mater Chem. 2011;21(48):19344-52.

[7] Tang L, Zhang J, Tang Y, Zhou Y, Lin Y, Liu Z, et al. Fluorine/adamantane modified cyanate resins with wonderful interfacial bonding strength with PBO fibers. Composites Part B: Engineering. 2020;186:107827.

[8] Liu Z, Fan X, Zhang J, Chen L, Tang Y, Kong J, et al. PBO fibers/fluorine-containing liquid crystal compound modified cyanate ester wave-transparent laminated composites with excellent mechanical and flame retardance properties. J Mater Sci Technol. 2023;152:16-29.

[9] Zhou YX, Zhang JL, Qu C, Li LC, Kong J, Gu JW. Synchronously improved wave-transparent performance and mechanical properties of cyanate ester resins via introducing fluorine-containing linear random copolymer. Adv Compos Hybrid Ma. 2021;4(4):1166-75.

[10] Liu R, Yan HX, Zhang YB, Yang KM, Du S. Cyanate ester resins containing Si-O-C hyperbranched polysiloxane with favorable curing processability and toughness for electronic packaging. Chem Eng J. 2022;433.

[11] Liu Z, Fan X, Han M, Li H, Zhang J, Chen L, et al. Branched fluorine/adamantane interfacial compatibilizer for synchronously enhancing interlaminar shear strength and wave-transparent performances of PBO fibers/cyanate ester laminated composites.

Chinese Journal of Chemistry. 2023.

[12] Tang L, Dang J, He MK, Li JY, Kong J, Tang YS, et al. Preparation and properties of cyanate-based wave-transparent laminated composites reinforced by dopamine/POSS functionalized Kevlar cloth. Compos Sci Technol. 2019;169:120-6.

[13] Liu Z, Fan X, Han M, Zhang J, Chen L, Tang Y, et al. Significantly improved interfacial properties and wave-transparent performance of PBO fibers/cyanate esters laminated composites via introducing a polydopamine/ZIF-8 hybrid membrane. Compos Sci Technol. 2022;223:109426.

[14] Zhang J, Liu Z, Han M, Zhang J, Tang Y, Gu J. Block copolymer functionalized quartz fibers/cyanate ester wave-transparent laminated composites. J Mater Sci Technol. 2023;139:189-97.